Journal of the Geological Survey of Brazil

Geochemical and isotopic constraints on the petrogenesis of the Cretaceous alkaline Morro Redondo intrusive complex, Rio de Janeiro, Brazil: implications for alkaline magma genesis

Carlos Eduardo Mota[1], Arthur de Melo Said Fabião Moreira da Silva[2], Fred Jourdan[3], Mauro Cesar Geraldes[4], Guilherme Loriato Potratz[2*]

[1]Geological Survey of Brazil-CPRM, Av. Pasteur, 404, Urca, Rio de Janeiro-RJ, Brazil, CEP 22290-255
[2]Postgraduate Program in Geosciences, Rio de Janeiro State University. Rua São Francisco Xavier, 524, Rio de Janeiro - RJ - CEP: 20550-900
[3]Western Australian Argon Isotope Facility, John de Laeter Centre & School of Earth and Planetary Sciences, Curtin University, Building 301, Australia
[4]Department of Mineralogy and Igneous Petrology. Rio de Janeiro State University. Rua São Francisco Xavier, 524, Rio de Janeiro - RJ - CEP: 20550-900

Abstract

The Morro Redondo Complex is composed of plutonic and volcanic alkaline rocks. This igneous complex is part of the Poços de Caldas - Cabo Frio Magmatic Alignment (PCCFA). This study aims to contribute to the understanding of the petrogenesis of the rocks in the Morro Redondo complex and, thereby, contribute to the debate on the genesis of the PCCFA. In this work, we conducted analyses of whole-rock geochemistry, $^{40}Ar/^{39}Ar$ thermochronology, U-Pb geochronology on zircon grains, and Rb-Sr, Sm-Nd, and Lu-Hf isotopic analyses. Four distinct lithotypes are present: nepheline syenites, alkali feldspar syenites, trachytes, and phonolites. The rocks of the Morro Redondo complex are miaskitic, have intermediate values of SiO_2, and show significant crustal assimilation, mainly observed in the relationship between the SSI and (Na+K)/Al indices, together with the Hf isotopic signature. A hornblende crystal obtained from a sample of nepheline syenite provided a plateau age of 74.35 ± 0.50 Ma. The initial ratios of $^{87}Sr/^{86}Sr$ range from 0.70565 to 0.71042, and the initial ratios of $^{143}Nd/^{144}Nd$ range from 0.51234 to 0.5124. Hf data suggest a hybrid origin for the Morro Redondo complex, with sources from both crustal and mantle origins. The data obtained indicate that at least three magmatic pulses contributed to the formation of the Morro Redondo complex, with the participation of both crustal and mantle sources, generating magmas of miaskitic affinity.

Article Information

Publication type: Research Article
Received 17 October 2023
Accepted 15 March 2024
Online pub. 20 March 2024
Editor: Chris Harris

Keywords:
Geochemistry
$^{40}Ar/^{39}Ar$
U-Pb
Lu-Hf
Crustal assimilation
miaskitic rocks

*Corresponding author
Guilherme Loriato Potratz
E-mail address: geo.loriato@gmail.com

1. Introduction

According to Almeida (1971, 1972), the Brazilian platform possesses dozens of alkaline bodies of Mesozoic and Cenozoic age. Riccomini et al. (2005) proposed grouping these alkaline bodies into 15 provinces based on petrographic, geochronological, geochemical, and tectonic data. Among the 15 suites proposed by Riccomini et al. (2005), we highlight the Poços de Caldas – Cabo Frio Magmatic Alignment (PCCFA). The PCCFA is a magmatic province oriented WNW-ESE, which extends for approximately 1150 km (Melluso et al. 2017; Gomes and Comin-Chiaramonti 2005; Riccomini et al. 2005).

Two models remain debated for the PCCFA genesis and the Cretaceous alkaline magmatism. One model correlates the emplacement of alkaline bodies with the reactivation of sub-crustal faults, lithospheric fertilization, and magma ascent through fracture zones (Almeida 1991; Ferrari 2001; Alves et al. 2006; Riccomini et al. 2005; Zalán and Oliveira 2005). The other model relates alkaline magmatism with Hotspot activity and suggests that the alignment of intrusions results from the relative movement between the South American plate and the mantle plume (Sadowski and Dias Neto 1981; Thomaz Filho et al. 2005; Thompson et al. 1998; VanDecar et al. 1995). The second model is strongly supported by the decrease, although not linear, from west to east of the ages of alkaline bodies (Thomaz Filho et al. 2005).

ISSN: 2595-1939
https://doi.org/10.29396/jgsb.2024.v7.n2.1
Open access at https://jgsb.sgb.gov.br

Given that the debate on the genesis of the PCCFA remains open, we will present information on the Morro Redondo Complex in this work. This alkaline body belongs to the magmatic alignment. In this contribution, we constrain the formation processes (petrogenesis) and sources of alkaline magmatic rocks from the Cretaceous Morro Redondo Complex, part of the PCCFA, using geochemistry and isotopic data (U-Pb, Lu-Hf, Sm-Nd, Rb-Sr and $^{40}Ar/^{39}Ar$).

2. Geological Setting

The Poços de Caldas – Cabo Frio Alignment (PCCFA) was defined by Riccomini et al. (2005) as an alkaline province trending WNW-ESE with a slightly curved shape (Figure 1). The alignment is characterized by a series of intrusive, hypabyssal, and extrusive alkaline bodies, predominantly comprising nepheline syenites, syenites, phonolites, and trachytes (Almeida et al. 1996; Motoki et al. 2008; Riccomini et al. 2005). From east to west (Figure 1), the main alkaline bodies are Poços de Caldas, Passa Quatro, Itatiaia, Morro Redondo, Tinguá, Mendanha, Itaúna, Tanguá, Rio Bonito, Soarinho, Morro dos Gatos, Morro de São João, and Ilha do Cabo Frio.

Brotzu et al. (2005) considered that alkaline syenites and nepheline syenites are the main constituents of the alkaline bodies; however, in some intrusive complexes, quartz syenites and granites occur, such as Soarinho and Itatiaia. Associated with the igneous complexes are alkaline composition dikes related to the ENE-EW fault system (Brotzu et al. 2005). The ages of the Poços de Caldas – Cabo Frio Alignment bodies vary decreasingly from east to west between 84 and 39 Ma, although not linearly (Santos and Hackspacher 2021). It is worth mentioning that most alkaline bodies of the PCCFA tend to intrude Neoproterozoic sin-, late- or post-collisional granites and syenites from the Brasília and Ribeira belts (Valeriano et al. 2011; Tupinambá et al. 2012; Rosa and Ruberti 2018).

3. Materials and methods

3.1. Geochemistry

Samples selected for geochemical analysis were analyzed at the ACTLABS laboratory in Canada. The analytical techniques included atomic emission spectrometry (ICP-AES) for oxides. X-ray fluorescence in fused pellets for trace elements, S, Cl, Rb, Sr, Ba, and Zr, atomic absorption spectrometry for determining Mn, Mg, Na, K, Cu, Mo, Sn, and Pb elements. Optical spectrometry for trace elements Nb, Y, Ni, and V, and rare earth elements (REE) were analyzed by mass spectrometry (ICP-MS).

3.2. Rb-Sr and Sm-Nd isotopes

Samples for Sr and Nd isotopes were analyzed at the

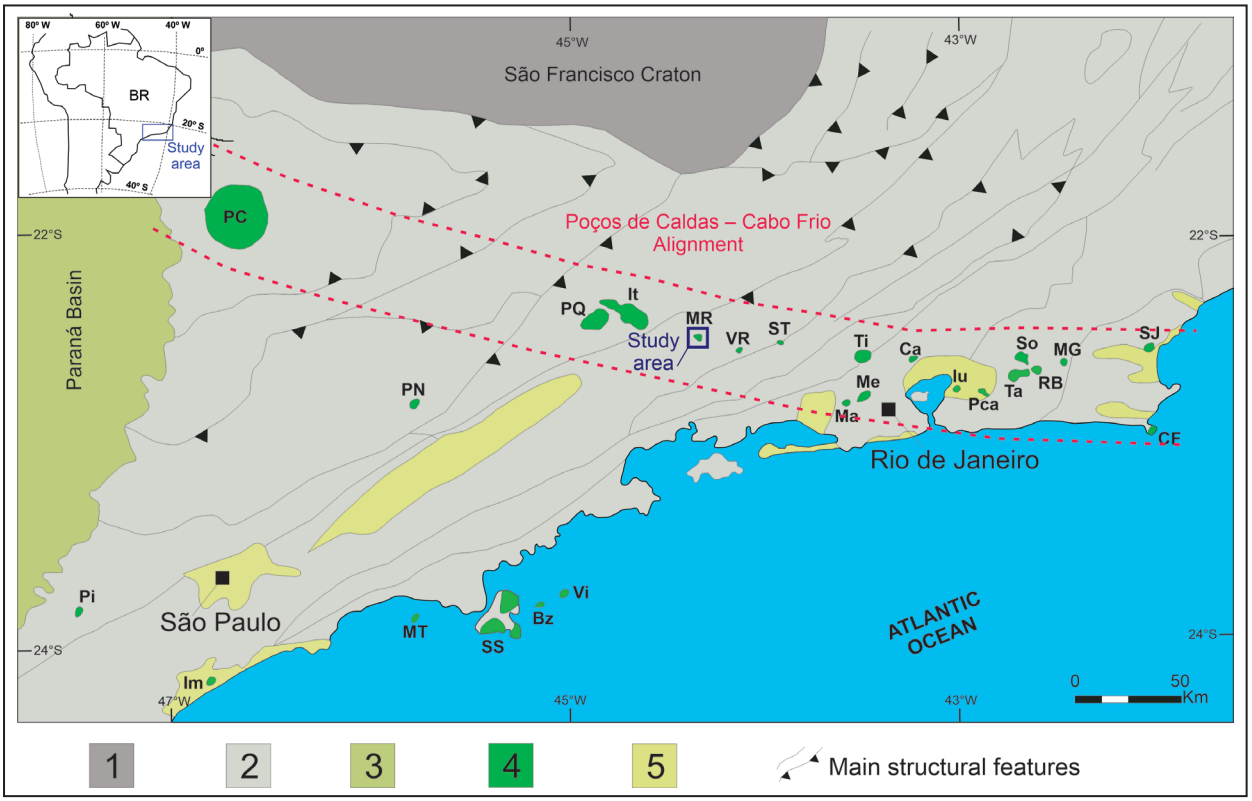

FIGURE 1. Distribution of alkaline bodies in southeastern Brazil, highlighting the Poços de Caldas – Cabo Frio Magmatic Alignment (highlighted by dashed red lines). The blue rectangle highlights the study area of this work. Legend: 1 – São Francisco Craton; 2 – Brazilian mobile belts (Ribeira and Brasília); 3 – Paraná Basin; 4 – Alkaline occurrences of the Cretaceous and Tertiary; 5 – Cenozoic sediments and Paleozoic coverings. Poços De Caldas – Cabo Frio Alignment: PC – Poços de Caldas; PQ – Passa Quatro; It – Itatiaia; MR – Morro Redondo (study area); VR – Volta Redonda; ST – Serra dos Tomazes; Ti – Tinguá; Me – Mendanha; Ma – Marapicú; Iu – Itaúna; Pca – Porto das Caixas; Ta – Tanguá; So – Soarinho; RB – Rio Bonito; MG – Morro dos Gatos; SJ – Morro de São João; CF - Cabo Frio. Other alkaline bodies in southeastern Brazil: Pi – Piedade; PN – Ponte Nova; MT – Ilha Monte de Trigo; SS – Ilha de São Sebastião; Bz – Ilha dos Búzios; Vi – Ilha de Vitória. Adapted from Gomes and Comin-Chiaramonti (2005).

Isotopic Geochronology Laboratory of the UNB Geosciences Institute. For Sm-Nd and Rb-Sr analysis, pulverized rocks were dissolved in hydrofluoric acid (HF). For Sm-Nd, the ^{145}Nd and ^{144}Sm tracers were added to the solutions. No tracers were added for Rb-Sr analyses and the natural isotopic composition was analyzed.

The rare earth elements were separated by cation exchange columns with resin. Isotopic concentrations of these elements were measured by TIMS (thermo ionization mass spectrometer) on the Finnigan multi-collector spectrometer. The data obtained include absolute amounts of samarium and neodymium, isotopic ratios ^{147}Sm/^{144}Nd, ^{143}Nd/^{144}Nd, and ^{87}Sr/^{86}Sr, For the calculations of isotopic ratios, the εNd parameter, and the TDM model age, the following constants were used: ^{146}Nd/^{144}Nd = 0.7219 and λSm = 0.654 x 10-11 year-1, in addition to the average value of 0.512371 for ^{146}Nd/^{144}Nd in the depleted mantle, with an average extraction age of 0.79 Ga (DePaolo 1988).

3.3. ^{40}Ar/^{39}Ar Thermochronology

We separated unaltered, optically transparent, 250-315 μm-size hornblende crystals from sample MRD-01. The hornblende crystals were separated using a Frantz magnetic separator, and then carefully hand-picked under a binocular microscope. The selected hornblende minerals were further leached in diluted HF for one minute and then thoroughly rinsed with distilled water in an ultrasonic cleaner.

Samples were loaded into a large well of a 1.9 cm diameter and 0.3 cm depth aluminum disc. These wells were bracketed by small wells that included Fish Canyon sanidine (FCs) used as a neutron fluence monitor for which an age of 28.294 ± 0.036 Ma (1σ) was adopted (Renne et al. 2011). The discs were Cd-shielded (to minimize undesirable nuclear interference reactions) and irradiated for 25 hours in the Hamilton McMaster University nuclear reactor (Canada) in position 5C. The mean J-values computed from standard grains within the small pits and determined as the average and standard deviation of J-values of the small wells for each irradiation disc is given along with the raw data.

Mass discrimination is given in Annex for each sample and was monitored using an automated air pipette and calculated relative to an air ratio of 298.56 ± 0.31 (Lee et al. 2006). The correction factors for interfering isotopes were (^{39}Ar/^{37}Ar)Ca = 7.30x10-4 (± 11%), (^{36}Ar/^{37}Ar)Ca = 2.82x10-4 (± 1%) and (^{40}Ar/^{39}Ar)K = 6.76x10-4 (± 32%).

The ^{40}Ar/^{39}Ar analyses were performed at the Western Australian Argon Isotope Facility at Curtin University. The sample was step-heated in a double vacuum high frequency Pond Engineering© furnace. The gas was purified in a stainless-steel extraction line using two AP10 and one GP50 SAES getters and a liquid nitrogen condensation trap. Ar isotopes were measured in static mode using a MAP 215-50 mass spectrometer (resolution of ~400; sensitivity of 4x10-14 mol/V) with a Balzers SEV 217 electron multiplier mostly using 9 to 10 cycles of peak-hopping.

The data acquisition was performed with the Argus program written by M.O. McWilliams and ran under a LabView environment. The raw data were processed using the ArArCALC software (Koppers 2002) and the ages have been measured using the decay constant of Renne et al. (2010) and later re-calculated using the decay constants recommended by Renne et al. (2011). Blanks were monitored every 3 to 4 steps and typical 40Ar blanks range from 1 x 10-16 to 2 x 10-16 mol. Our criteria for the determination of plateau are as follows: plateaus must include at least 70% of ^{39}Ar. The plateau should be distributed over a minimum of 3 consecutive steps agreeing at 95% confidence level and satisfying a probability of fit (P) of at least 0.05. Plateau ages are given at the 2σ level and are calculated using the mean of all the plateau steps, each weighted by the inverse variance of their individual analytical error. Inverse isochrons include the maximum number of steps with a probability of fit ≥ 0.05. ^{40}Ar/^{36}Ar intercept values are provided. All sources of uncertainties are included in the calculation and have been calculated using a Monte Carlo approach following Renne et al. (2010).

3.4. U-Pb Ages

U-Pb analyses were performed at the UERJ MultiLab laboratory using laser-induced plasma mass spectrometry (LA-ICP-MS), and the apparatus used was Thermo Scientific's Neptune. The results are presented in Concordia Tera and Wasserburg (1972) diagrams built with the ISOPLOT program (Ludwig 2003).

The laser spot diameter used in the analysis of Morro Redondo samples were between 30 and 50μm and it was set at a frequency of 10Hz. Four Soarinho intrusion samples were selected for U-Pb dating. The larger-than-usual spot diameter and higher laser power are justified by the low Pb concentration of some zircon grains (<20 ppm), and this procedure improved readability and data quality.

The standard U-Pb analysis procedure performed on the MultiLab in each analysis block was as follows: it started with the blank analysis, then the GJ1 standard was analyzed, and then nine analyzes were performed on the sample zircons, followed by one analysis of the 91500-reference material, another analysis of the GJ1 reference material, ending each battery with another analysis.

3.5. Lu-Hf isotopes

The systematics of Lu-Hf in zircon grains is of particular interest as Hf is present in the chemical composition of zircon characterized by high Hf contents and low Lu values so that Hf radioactive decay corrections are negligible. This particularity makes the Lu-Hf system ideal for isotopic investigations of rocks over 3Ga (Vervoort and Patchett 1996).

The ^{176}Hf/^{177}Hf ratio of the chondritic reservoir (CHUR) is said to represent the undifferentiated material of the early solar system (solar nebula) and was established through the isotopic Lu-Hf ratio of the chondrites (Blichert-Toft and Albarède 1997). The temporal variation of the CHUR ^{176}Hf/^{177}Hf ratio is given by the ratios of ^{176}Lu/^{177}Hf (0.0332 ± 2) and ^{176}Hf/^{177}Hf (0.282772 ± 29) ratios (Machado and Simonetti 2001). This corresponds to an initial ^{176}Hf/^{177}Hf ratio of 0.279742 ± 29 for a 4.56 Ga solar system. Samples derived from the depleted mantle will have, relative to CHUR at time (t), εHf with positive values or negative if derived from the crust. The recent introduction of MC-ICPMS (a multi-collector ICP-MS) has allowed the routine use of Lu-Hf, requiring little sample for its isotopic analysis and with high precision and efficiency. The plasma source (from ICP) allows for more efficient ionization for analysis than other spectrometric equipment.

4. Results

4.1. Local geology

The Morro Redondo Alkaline Complex has an approximately elliptical shape and an area of approximately 9 km². The complex is intruded in orthogneisses and paragneisses, with contacts that could not be defined due to the density of the local vegetation. The distribution of field points for outcrop description and sample collection is presented on the geological map (Appendix 1). The complex is mainly composed of plutonic rocks (Figure 2) of syenitic composition, with variation in grain size and nepheline content. In addition to plutonic rocks, occasional trachyte and phonolite were observed (Figure 2). The plutonic lithotypes observed were nepheline syenite and alkali feldspar syenite. Given the scarcity of outcrops and the advanced degree of weathering, it was impossible to determine the contact relationships between the observed lithologies.

Nepheline syenites show inequigranular texture, with grain size ranging from medium to coarse and an abrupt transition between different grain sizes (Figure 2). They are composed of approximately 55% K-feldspar, 30% nepheline, 8% hornblende, 4% biotite, 3% plagioclase, and, in modal proportions less than 1%, zircon, titanite, apatite, and opaque minerals. K-feldspar crystals are generally euhedral, occasionally exhibiting perthitic texture. Some hornblende grains display biotite reaction on borders (Figure 3). Nepheline is anhedral and exhibits alteration rims to cancrinite, sericite, and carbonate.

Alkali feldspar syenites have a medium grain size and light gray color (Figure 2), predominating in the southern portion of the igneous complex. The composition of these rocks is approximately 75% alkali feldspar, 20% hornblende, 3% titanite, and the remaining 2% corresponds to plagioclase, biotite, nepheline, opaque minerals, apatite, and zircon. K-feldspar crystals are anhedral to subhedral and rarely exhibit perthitic texture. Hornblende and titanite occur as euhedral to subhedral crystals (Figure 3).

Trachytes are light gray to gray with a porphyritic texture, with about 5 to 10% K-feldspar phenocrystals. In addition to the phenocrystals, it is possible to observe the presence of approximately 3 mm diameter (Figure 2) vesicles filled with iron oxide. The matrix comprises K-feldspar microliths with disseminated clay, iron oxides, opaque minerals, and apatite. Iron oxide pseudomorphs primary K-feldspar, which is also in the process of kaolinization. K-feldspar microlites are covered by hydrothermal sericite. The presence of polygonal and millimeter-sized xenoliths of granitic and syenitic composition rocks with rounded corners was observed. Phonolite blocks were observed at only one point (MRD-11). The rocks are gray and have a texture characterized by the intertwined

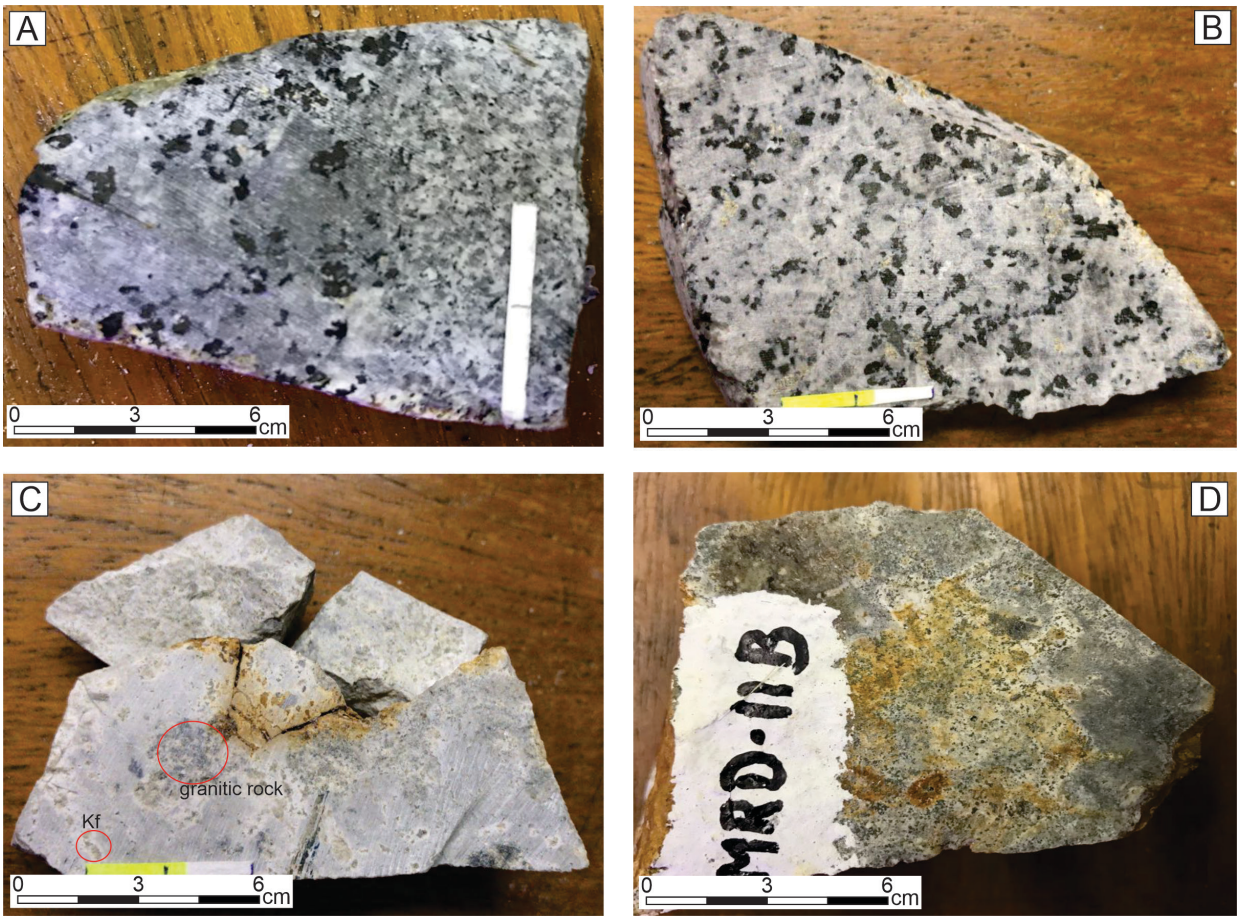

FIGURE 2. Samples of rocks found in the Morro Redondo complex. A presents a sample of nepheline syenite, where it is possible to observe the variation in the rock's grain size [there is also a finer grained right hand part]. B presents a sample of alkali feldspar syenite with medium grain size. In C, we present a sample of trachyte, where it is possible to observe feldspar phenocrysts and fragments of rocks with granitic composition. In Figure D, we present a sample of phonolite.

arrangement of very fine-grained crystals (phonolitic texture) (Figure 3).

4.2. Major and trace elements

Lithogeochemical data and CIPW norms for the Morro Redondo are presented in the Electronic Supplementary Material A (ESM-A). The data presented in this work were separated into plutonic and volcanic groups. The two groups are intermediate in terms of SiO_2 concentration. In the group of plutonic rocks, the SiO_2 concentration varies between 54.98 and 58.88% by weight, with a standard deviation of 1.27. In the group of volcanic rocks, the SiO_2 concentration varies between 54.93 and 59.31% by weight, with a standard deviation of 1.27.

Figure 4 demonstrate the behavior of the oxides in the two groups of rocks. Like volcanic rocks, plutonic rocks are enriched in Fe_2O_3, CaO, MgO, TiO_2, P_2O_5, and MnO (Figures 4). Volcanic rocks are enriched, about plutonic rocks, in Al_2O_3 and Na_2O (Figures 4). The behavior of K_2O is similar

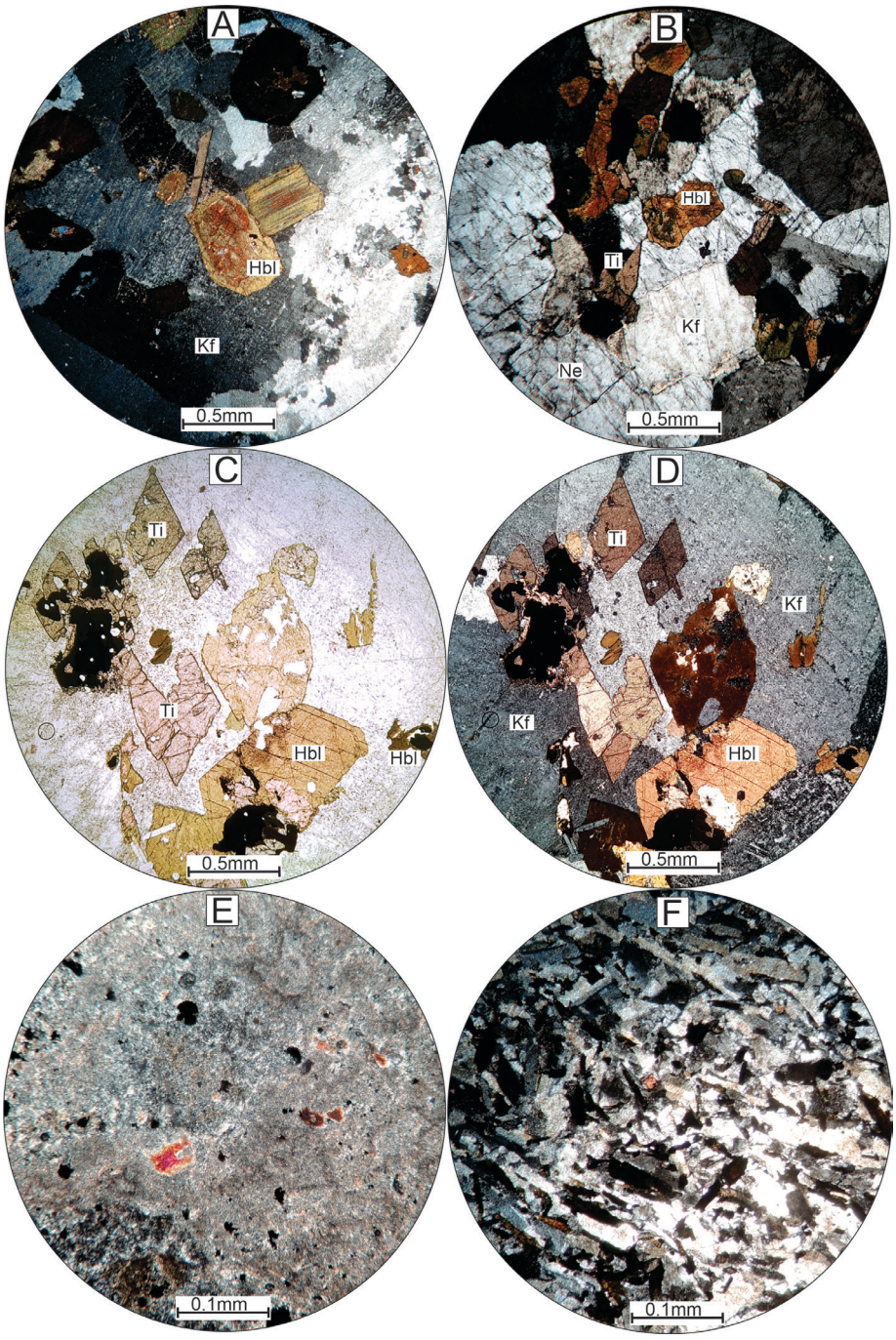

FIGURE 3. Photomicrographs of the rocks of the Morro Redondo complex. Figures A and B show photomicrographs (plane-polarized light) of nepheline syenites, where the change of hornblende crystals to biotite is observed. In Figure C (natural light) and D (plane-polarized light), euhedral/subhedral crystals of titanite and hornblende are observed. Figure E presents a photomicrograph of a trachyte sample. Figure F presents a photomicrograph of a phonolite sample. Legend: Kf - K-feldspar; Hbl - Hornblende; Ti - Titanite; Ne – Nepheline.

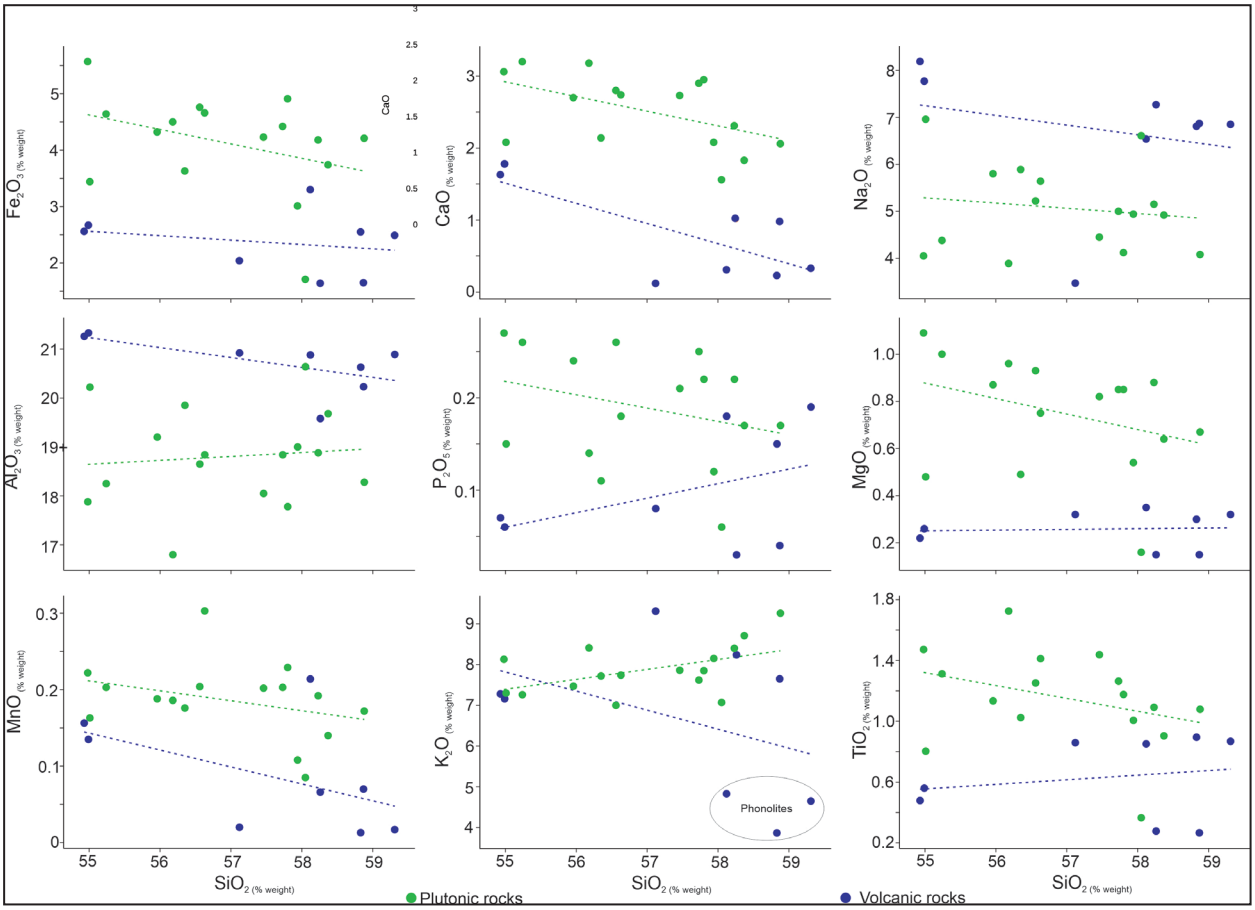

FIGURE 4. Harker diagrams demonstrating the variation of oxides in plutonic (green markers) and volcanic (purple markers) rock groups. The dotted lines indicate the linear trend of the oxides about SiO2. The dotted ellipse in the K2O vs SiO2 diagram highlights three samples of phonolites whose behavior stands out from other rocks (volcanic and plutonic).

in both groups, demonstrating enrichment to SiO_2, except for three phonolite samples, which present lower values in K_2O concentration (Figure 4).

The volcanic rocks were classified into phonolites and trachytes according to the chemical classification of Le Bas et al. (1986) (Figure 5-A). The A/NK vs A/CNK diagram demonstrates the metaluminous character of plutonic rocks, the peraluminous character of trachytes, and the transition between the peralkaline and metaluminous fields for phonolites (Figure 5-B). The difference between phonolites and trachytes is also observed in the normative composition, where trachytes stand out due to the presence of normative quartz and corundum ((ESM-A)).

Both volcanic and plutonic rocks present a similar pattern in the multi-element diagram (normalized by the primitive mantle (Figures 6-A and B). In both groups of rocks, negative anomalies of Ba, P, and Ti and concentrations close to those of the primitive mantle are observed for Lu, Yb, Y, Dy, and P. Trachytes. Phonolites present a subtle difference in relative enrichment, with phonolites slightly more enriched about the primitive mantle (Figure 6-A). Among volcanic rocks, the same pattern of relative enrichment is observed in rare earth elements (Figure 6-C). Phonolites are slightly more enriched than trachytes; however, both sets of rocks present enrichment of light rare earth about heavy ones. Plutonic rocks enrich light rare earths with heavy ones and positive Eu anomalies (Figure 6-D).

4.3. $^{40}Ar/^{39}Ar$ Thermochronology

The data from the diagrams presented in this section are provided in the Electronic Supplementary Material B. This section presents the plateau and isochrone ages obtained from a hornblende grain in sample MRD-01 (nepheline syenite). The plateau age obtained for the sample was 74.35 ± 0.5 Ma (MSWD = 0.74), including 100% of the released ^{39}Ar (Figure 7-A). The corresponding K/Ca ratios for each fusion step show that the values indicate a higher relative concentration of K in the first 2% of the sample (Figure 7-B). The inverse isochrone diagram is presented in Figure 8 and yielded an age of 74.23 ± 0.56 Ma (MSWD = 0.35) and an initial trapped $^{40}Ar/^{39}Ar$ ratio of 318 ± 45, indistinguishable from the atmospheric value.

4.4. U-Pb Geochronology

To obtain U-Pb ages in zircon grains, two samples of syenite (MRD-34B and MRD-35) and two samples of trachyte (MRD-33 and MRD-34A) were analyzed. No zircon grains were found in the phonolite samples. The results of the U-Pb analyses are shown in the Electronic Supplementary Material C. Figure 9 presents the cathodoluminescence images of the zircon grains analyzed in each sample, as well as the ages, Th/U ratios, and, when available, εHf values for each grain.

Sample MRD-33 (trachyte) yielded eight zircon grains, where 10 U-Pb analyses were conducted (Figure9-A). The

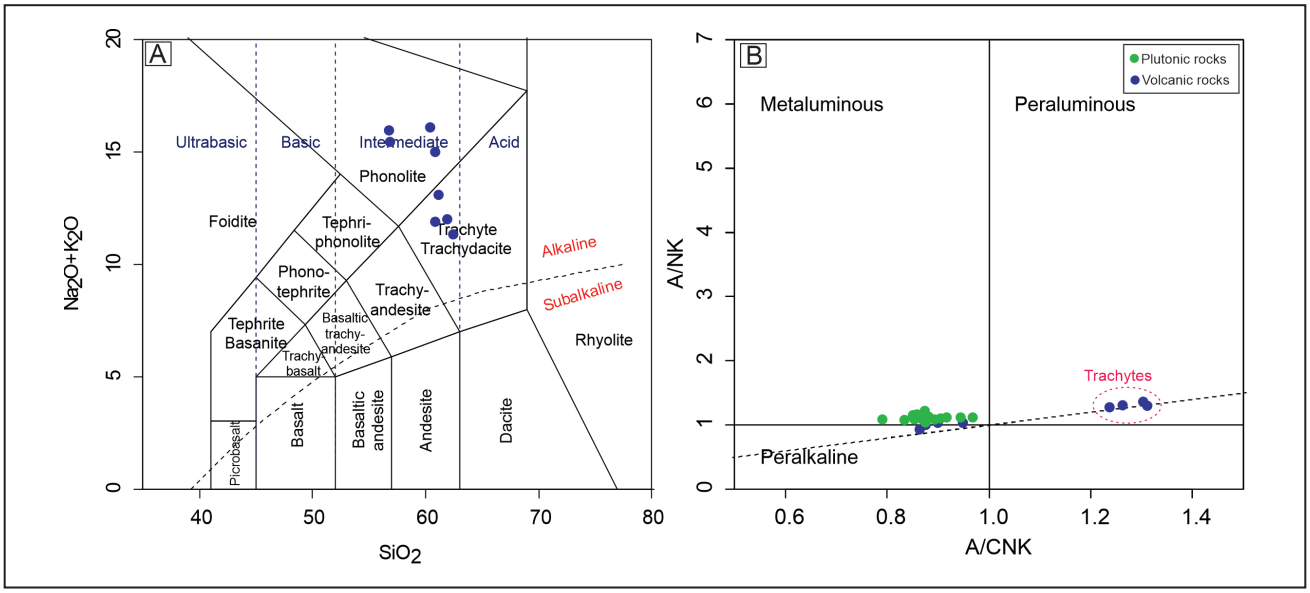

FIGURE 5. TAS Diagram of Le Bas et al. (1986) (A) and A/NK vs A/CNK diagram by Shand (1943) (B). Figure A, only the volcanic rocks are plotted.

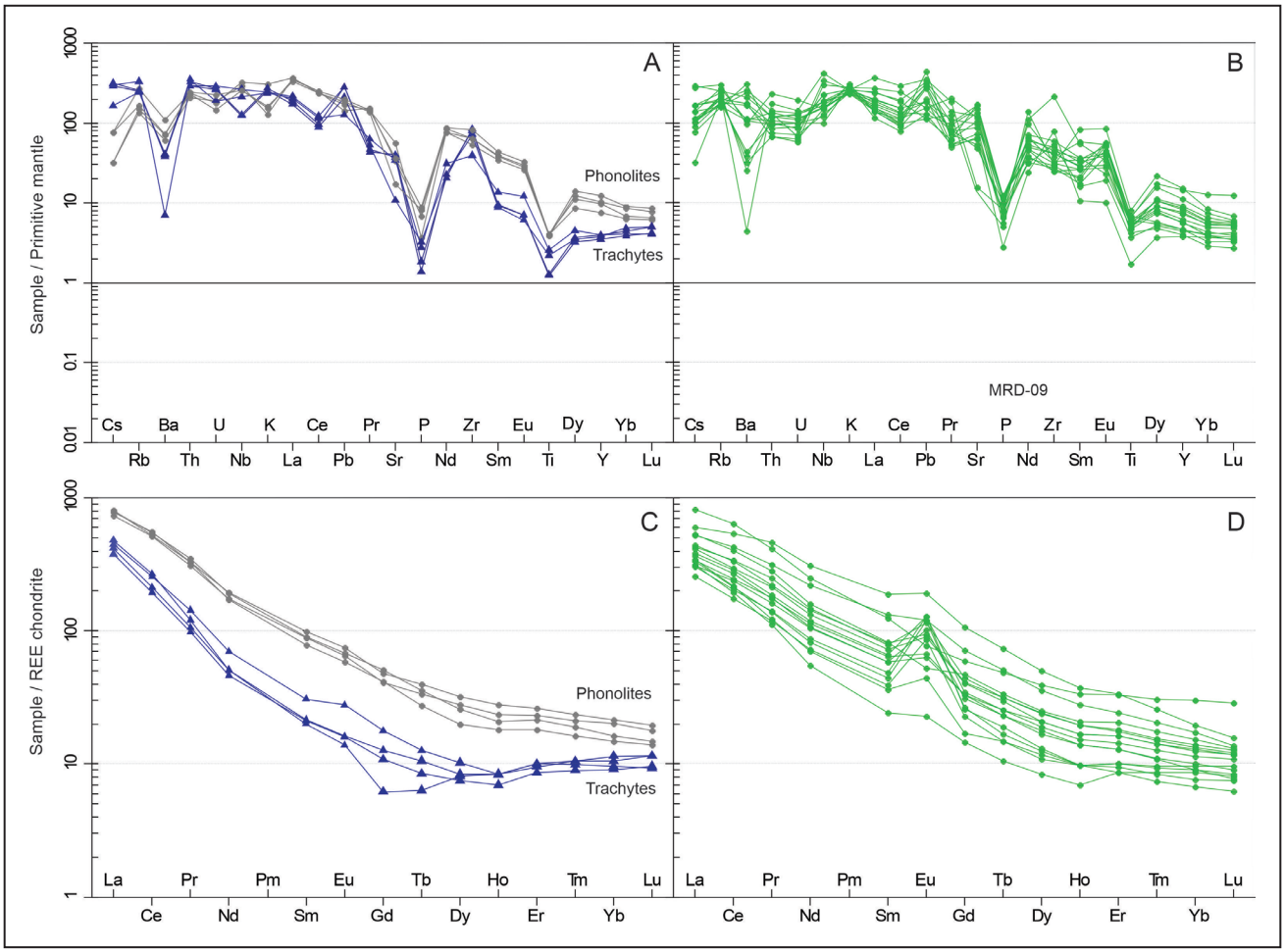

FIGURE 6. Standardized multi-element diagrams. Figures A and B present the normalized elements for the primitive mantle based on data from Sun and McDonough (1989). In A the volcanic rocks are plotted, subdivided into phonolites (gray) and trachytes (purple) and in B the plutonic rocks are plotted. Figures C and D show the rare earth elements normalized using the chondrite values of Boynton (1984). In C the volcanic rocks are subdivided into phonolites and trachytes and in D the plutonic rocks are plotted.

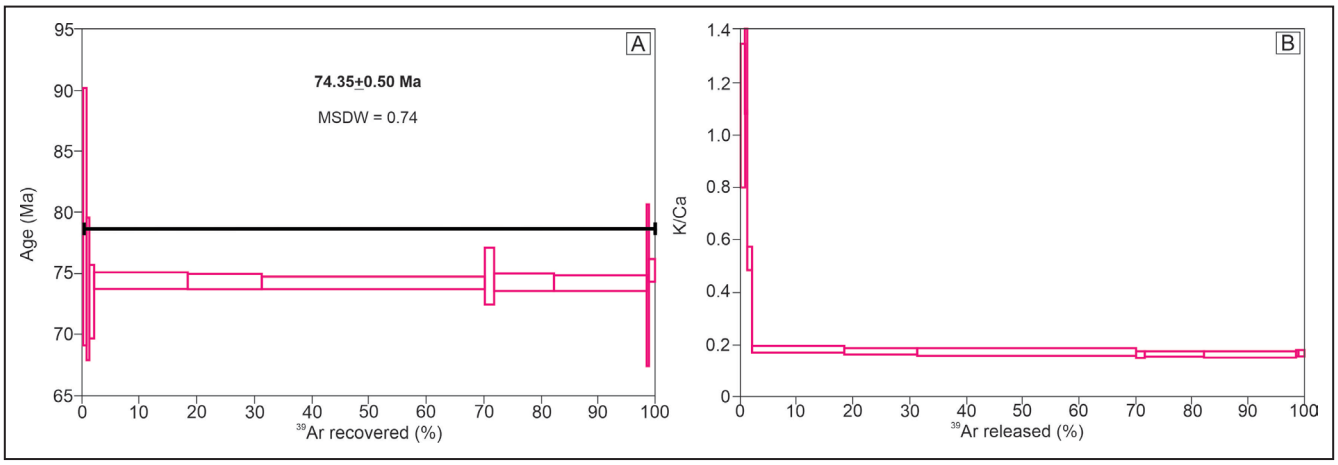

FIGURE 7. Plateau age obtained for a hornblende grain from sample MRD-01 (A), with an age of 74.35 ± 0.50 Ma and MSWD = 0.74. The K/Ca ratios obtained at each grain fusion step are presented on the right (B).

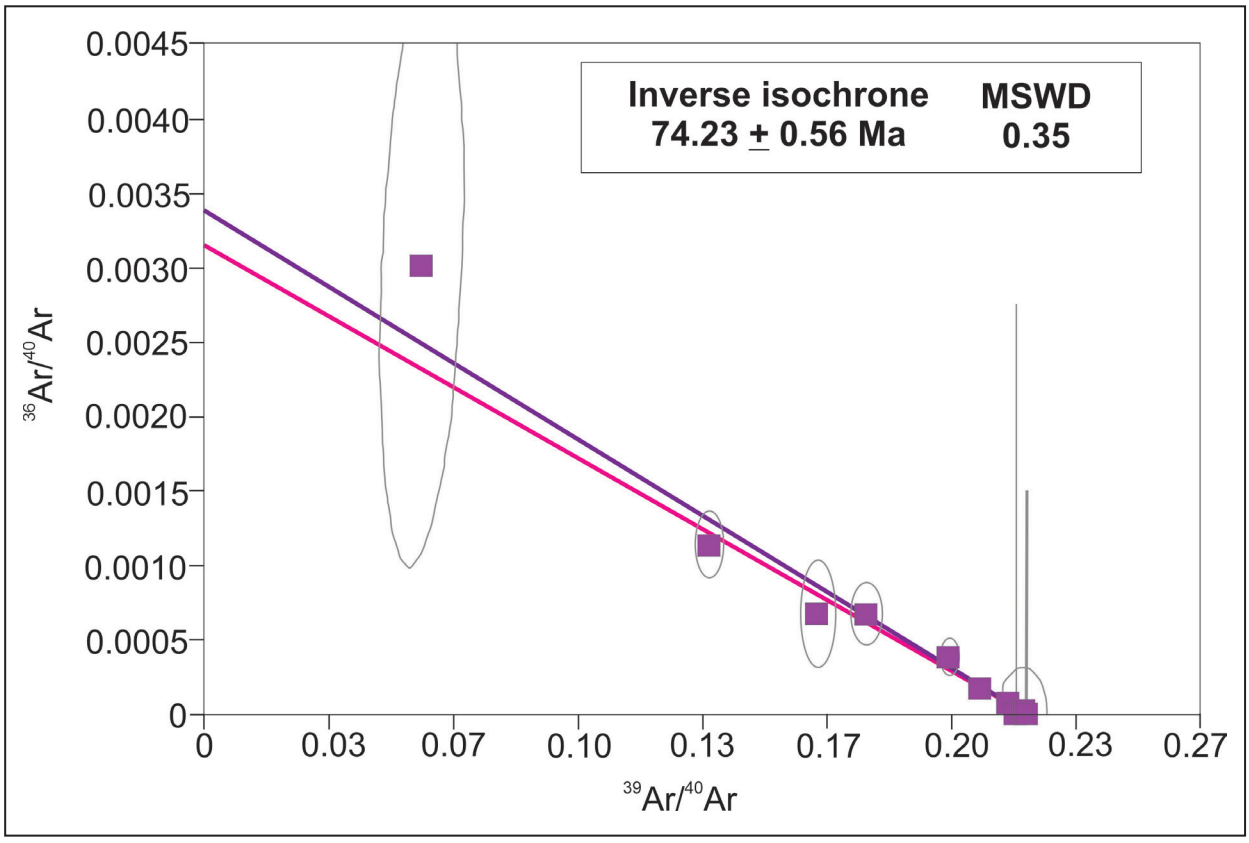

FIGURE 8. Isochrone diagram of $^{39}Ar/^{40}Ar$ for the hornblende grain from sample MRD-01. The pink line (bottom) intersects the y-axis at a fixed point, while the purple line (top) represents the real isochrone, calculated based on the data obtained in this work. The ellipses demarcate the errors on each analysis's x and y axes.

grains show zoned growth, apparently without modifications in growth directions, except for grain MRD 33 – 04, which exhibits homogeneous texture. Th/U ratios vary between 0.19 and 1.90. The ten analyses provided a lower intercept age of 77 ± 5 Ma (MSWD = 0.71) (Figure 10 – A). In sample MRD-34A (trachyte), only three zircon grains were obtained, where 7 U-Pb analyses were conducted (Figure 9-B). Zircon grains are homogeneous in this sample, and Th/U ratios vary between 1.63 and 2.68. The seven analyses yielded a lower intercept age of 76 ± 9 Ma (MSWD = 0.23) (Figure 10 – B).

Sample MRD-34B (syenite) yielded eight zircon grains, where 8 U-Pb analyses were conducted (Figure 9-C). The zircon grains from this sample exhibit compositional zoning and show no modifications in growth directions. Th/U ratios vary between 0.47 and 2.36. The eight analyses provided a lower intercept age of 74 ± 4 Ma (MSWD = 1.12) (Figure 10 – C). In sample MRD-35 (syenite), 12 zircon grains were obtained, where 15 U-Pb analyses were conducted (Figure

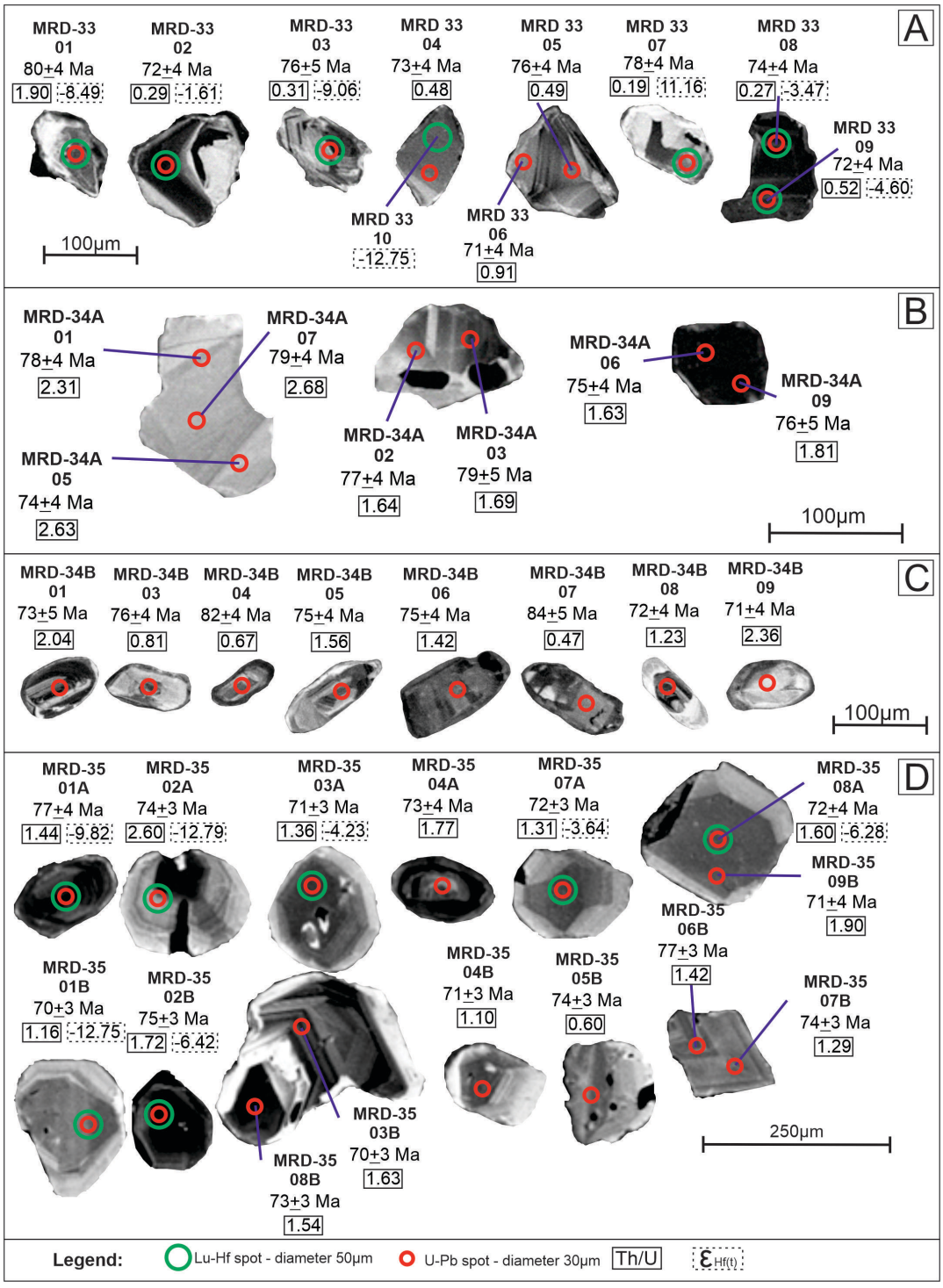

FIGURE 9. Cathodoluminescence images of the zircon grains analyzed in samples MRD-33 (A), MRD-34A (B), MRD-34B (C), and MRD-35 (D). The red (U-Pb) and green (Lu-Hf) circles indicate the position where the analyses were performed on each grain.

9-D). The zircon grains from this sample exhibit compositional zoning and show no modifications in growth directions. Th/U ratios vary between 0.60 and 2.60. The 15 analyses yielded a lower intercept age of 71 ± 4 Ma (MSWD = 0.46) (Figure 10 – D).

4.5. Rb-Sr and Sm-Nd isotopes

Isotopic analyses of Sr and Nd were performed on seven nepheline syenite samples, one phonolite sample, and one trachyte sample. The Sr and Nd isotopic data are presented in Table 1. The initial ratios of $^{143}Nd/^{144}Nd$ and $^{87}Sr/^{86}Sr$ were calculated based on the plateau age of 74.35 ± 0.50 Ma. The initial ratios of $^{87}Sr/^{86}Sr$ range from 0.70565 to 0.71042, and the initial ratios of $^{143}Nd/^{144}Nd$ range from 0.51234 to 0.5124, with εNd values ranging from -5.74 to -4.64.

4.6. Lu-Hf isotopes

Lu-Hf analyses were conducted on two samples (MRD-33 and MRD-35), both sienite samples. In each sample, analyses

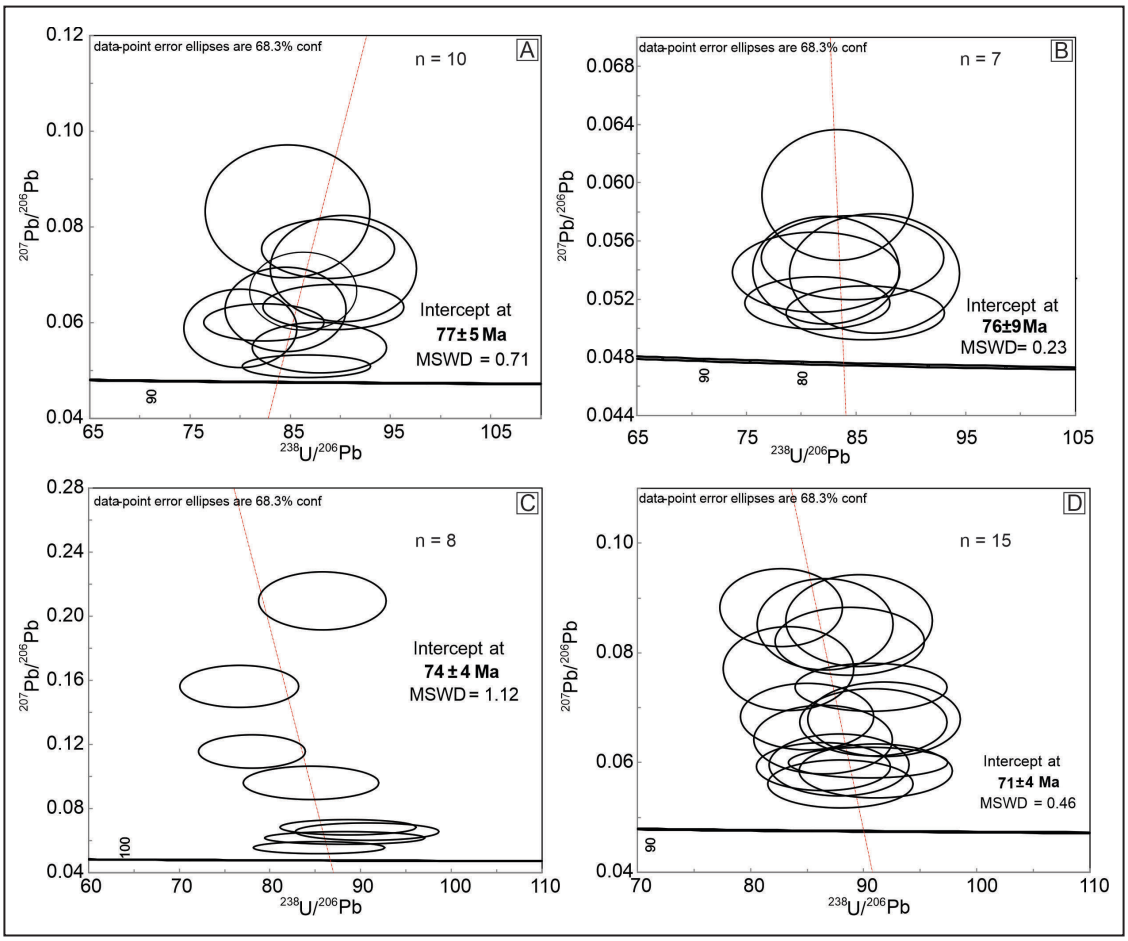

FIGURE 10. Tera-Wasserburg diagram showing the lower intercept ages for samples MRD-33 (A), MRD-34A (B), MRD-34B (C), and MRD-35 (D). The ellipses mark the errors on the x and y axes for each grain analyzed.

of 7 grains were utilized, with the remaining ones discarded due to being outside the quality standards adopted in this study. The analytical results are presented in the Electronic Supplementary Material D. The analyzed zircon grains are shown in Figure 9 (A and D).

Sample MRD-33 exhibits $^{176}Hf/^{177}Hf$ ratios ranging from 0.282376 to 0.283054, with the εHf parameter ranging from -12.75 to 11.21 (figure 11) and TDM ages ranging from 0.36 to 1.72 Ga. Sample MRD-35 shows $^{176}Hf/^{177}Hf$ ratios ranging from 0.282372 to 0.282636, with the εHf parameter ranging from -12.85 to -3.70 (figure 11) and TDM ages ranging from 1.20 to 1.72 Ga. The εHf values in range of -13 to 1, with only one positive value obtained in sample MRD-33.

5. Discussions

Despite the few observed contact relationships, the presence of plutonic and volcanic (sub-volcanic) rocks suggests that at least two magmatic pulses occurred to form the Morro Redondo complex. The syenites (nepheline- and alkali-feldspar) would represent the older pulse, and the trachytes and phonolites would represent the more recent pulse. The same pattern (plutonic rocks + volcanic rocks) is also observed in other alkaline bodies of the PCCFA, such as Poços de Caldas, Passa Quatro, Itatiaia, Tinguá, Mendanha, Tanguá, Rio Bonito, and Ilha de Cabo Frio (Amaral et al. 1967; Araujo 1995; Brotzu et al. 1992; Brotzu et al. 1997; Brotzu et al. 2007; Chiessi 2004; Enrich et al. 2005; Geraldes et al. 2013; Guarino et al. 2019; Montes-Lauar 1988; Mota et al. 2012; Motoki et al. 2012; Motoki et al. 2013; Sichel et al. 2008; Sígolo et al. 1992; Silva 2019; Silva et al. 2020; Vlach et al. 2018).

The presence of microxenoliths of syenitic composition in the trachytes reinforces the suggestion of at least two magmatic pulses. The presence of syenite microxenoliths demonstrates that rocks of syenitic composition had already crystallized at the time of the magmatic pulse that originated the trachytes. In addition, the presence of xenoliths of granitic composition demonstrates that fragments of country rocks were also incorporated into the magma of trachytic composition. The rocks classified in this study as trachytes may be related to the magmatic breccias reported by Brotzu et al. (1989). Another fact that corroborates at least two magma pulses is the coronas of biotite in hornblende crystals, which may have been formed by hydration reactions induced by fluids released by a new magmatic pulse after the crystallization of the syenites.

The mineralogical assemblage described in the syenites of the Morro Redondo complex is compatible with miaskitic rocks. Andersen et al. (2017) describe that in miaskitic rocks, Ti, Zr, and other HFSE elements are hosted in common minerals, such as ilmenite, titanite, and zircon, which is the

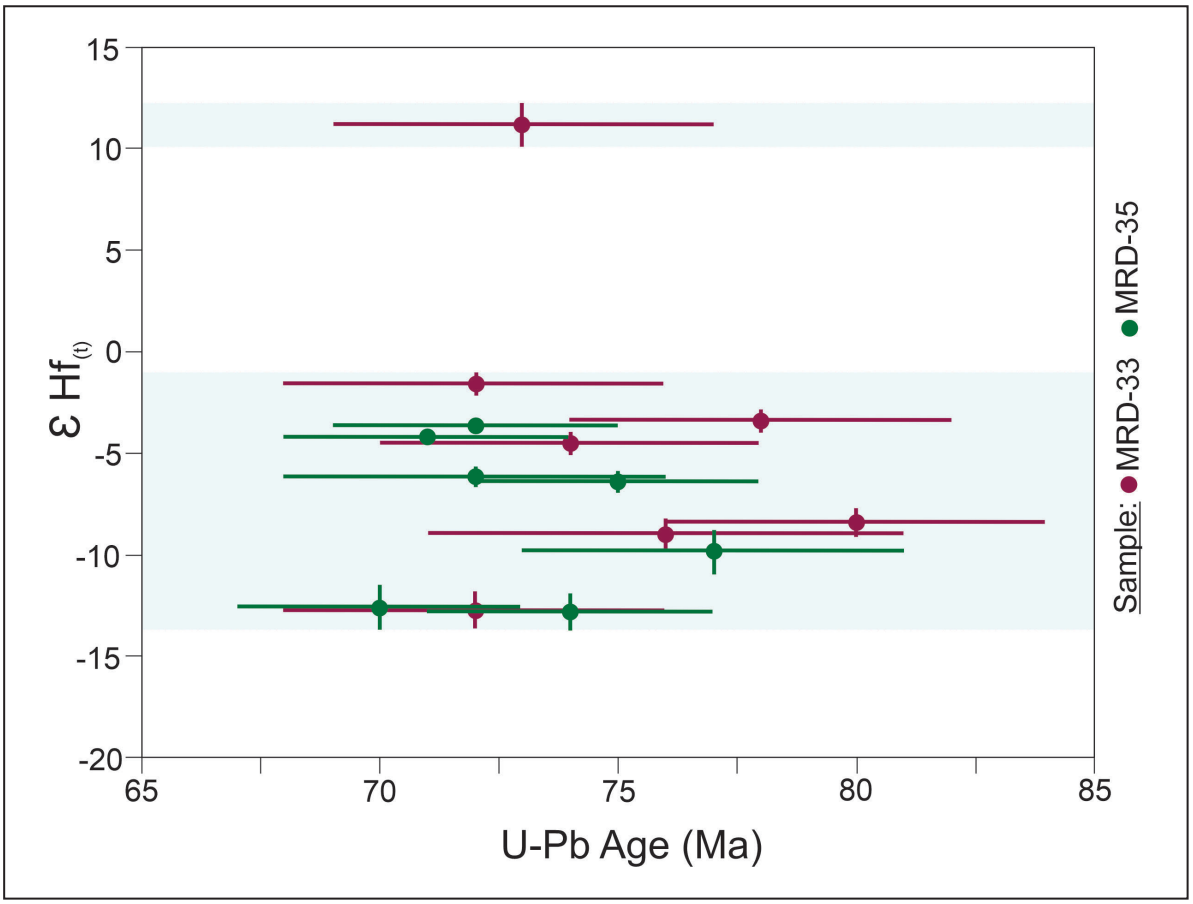

FIGURE 11. Scatter plot for U-Pb ages reported in $^{206}Pb/^{238}U$ and εHf calculated for the respective crystallization ages (U-Pb). Error bars are added for each axis.

Table 1: Sr and Nd isotopic data from the Morro Redondo alkaline intrusion rocks.

SAMPLE	Sm (ppm)	Nd (ppm)	$^{147}Sm/^{144}Nd$	$^{143}Nd/^{144}Nd \pm 2\sigma$	$\varepsilon_{Nd(i)}$	T_{DM} (Ga)	$^{87}Sr/^{86}Sr \pm 2\sigma$
MRD-01	7.657	51.200	0.0904	0.512369 + 15	-5.25	0.84	0.70757 ± 5
MRD-03	14.640	98.424	0.0899	0.512366 ± 16	-5.30	0.84	0.70628 ± 2
MRD-09	16.573	119.560	0.0838	0.512353 ± 15	-5.55	0.81	0.70624 ± 2
MRD-11D	17.048	131.868	0.0781	0.512399 ± 14	-4.66	0.73	0.70569 ± 3
MRD-12	9.634	66.050	0.0882	0.512356 ± 11	-5.49	0.84	0.70629 ± 3
MRD-20D	5.748	47.757	0.0728	0.512382 ± 12	-4.99	0.72	0.70603 ± 3
MRD-26	11.468	77.551	0.0894	0.512400 ± 11	-4.64	0.79	0.70592 ± 2
MRD-27	4.766	40.399	0.0713	0.512344 ± 15	-5.74	0.75	0.71042 ± 4
MRD-34B	8.851	60.609	0.0883	0.512379 ± 17	-5.04	0.81	0.70565 ± 2

case of the syenites of the Morro Redondo complex. According to Gomes and Comin-Chiaramonti (2005), miaskitic rocks are predominant in the continental alkaline magmatism of the southern region of the Brazilian platform.

Both plutonic and volcanic rocks have SiO_2 contents ranging from 54.93% to 59.31% (intermediate), demonstrating the absence of an expanded series in the Morro Redondo complex. The behavior of the oxides for the plutonic rocks shows low dispersion and moderately linear correlations concerning SiO_2 (see Harker diagrams), suggesting that fractional crystallization may have been the primary mechanism of magmatic differentiation. For the volcanic rocks, the data dispersion is high, making it difficult to define any magmatic process from the behavior of the oxides. However, in the parallel coordinate diagram, it is possible to observe that phonolites and trachytes exhibit distinct behavior regarding the main oxides.

The distinction between trachytes and phonolites is even more evident through the saturation of alkalis and alumina. The phonolites are at the transition between the peralkaline and

metaluminous fields (See Figure 6) and, in this sense, exhibit behavior like plutonic rocks. In contrast, the trachytes are essentially peraluminous (Figure 6). The distinction between trachytes and phonolites is also evident in the diagram of rare earth elements normalized by chondrite, where the phonolites are slightly more enriched than the trachytes.

Applying the silica saturation index (SSI) vs (Na/K)/Al(mol) diagram proposed by Motoki et al. (2010), the differentiation between trachytes and phonolites becomes even more evident (Figure 13). The trachyte samples plot close to the field of granites and gneisses, while the phonolites plot in the field of alkaline rocks or close to it. The plutonic rocks plot in the transition field between granites/gneisses and nepheline syenites, lying between the trachyte and phonolite samples. Analyzing the set of samples (plutonic + volcanic), they form a trend suggesting increased crustal contamination of an alkaline magma of origin. According to Motoki et al. (2010), the SSI vs. (Na/K)/Al(mol) diagram displays the assimilation of the continental crust through two thermodynamic incompatibilities: on the vertical axis, silica saturation; on the horizontal axis, alkali-alumina saturation.

According to Motoki et al. (2010), granites, gneisses, granodiorites (and other similar rocks) are subalkaline and supersaturated in silica, therefore plotting in the upper left quadrant (Figure 12). On the other hand, rocks such as nepheline syenites are typically peralkaline and undersaturated in silica, projecting in the lower right quadrant. A mixture of these components would form a negative correlation trend, as seen in Figure 12.

The absence of outcropping mafic rocks has complicated the understanding of possible sources and evolutionary processes of magmatism in the Morro Redondo complex. However, petrographic and geochemical information suggests that the differentiation process of plutonic rocks occurred through fractional crystallization with assimilation (AFC). Phonolites show a geochemical signature closer to the parental alkaline magma, while trachytes demonstrate significant crustal assimilation. Therefore, three distinct magmatic events are suggested: the emplacement of an alkaline magma in a magma chamber, which assimilates part of the country rocks and gives rise to plutonic rocks; the intrusion of phonolitic composition magmas; and the formation of trachytes, which may be related to the formation of the polymictic breccias described by Brotzu et al. (1989).

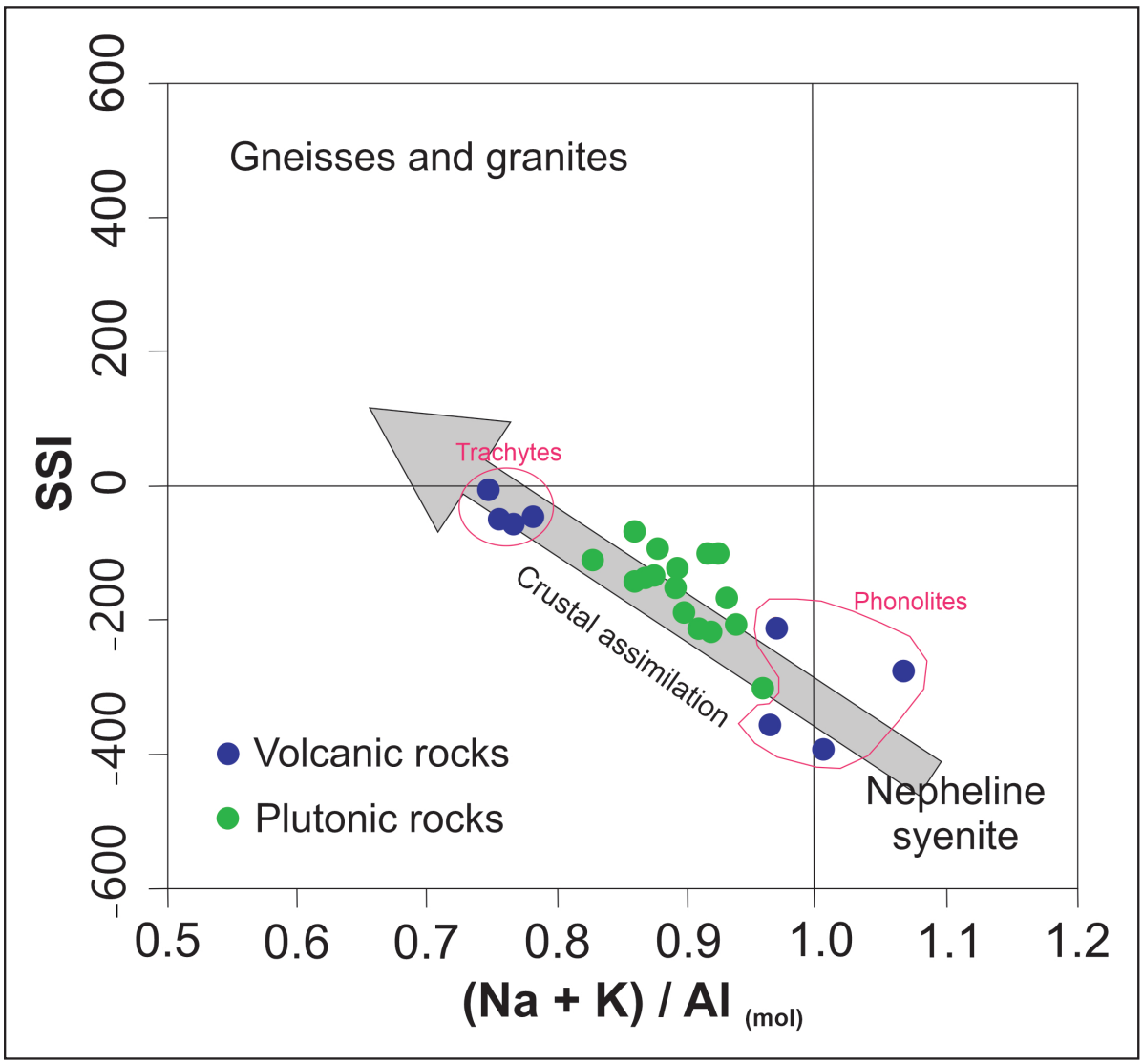

FIGURE 12. Plot of SSI vs. (NK)/Al (mol), with the proposed trend of crustal assimilation in the magmatism that gave rise to the Morro Redondo complex. Modified from Motoki et al. (2010).

The $^{40}Ar/^{39}Ar$ thermochronology results demonstrate relatively higher K concentrations in the first 2% of the sample. This may be related to the possibility of the edges of hornblende crystals being altered to biotite since biotite has more K in its composition/structure. The alteration process of hornblende is visible in the reaction coronas observed in thin sections.

We consider the age of 74.35 ± 0.5 Ma (plateau) as the best estimate for the crystallization of hornblende. The precision of U-Pb ages is lower than the plateau age ($^{40}Ar/^{39}Ar$); however, the absolute values are close to 74.35 ± 0.5 Ma. Despite the more significant margin of error, the U-Pb ages do not show evidence of a distinct magmatic event recorded by zircon grains; therefore, these grains possibly do not represent zircons that were incorporated during magma emplacement; a similar behavior was reported by Paquette and Mergoil-Daniel (2009) for the Central Massif of France.

The $^{147}Nd/^{146}Nd$ and $^{87}Sr/^{86}Sr$ ratios demonstrate that a group of samples presents isotopic signatures close to the composition of enriched mantle 1, with a tendency to deviate from this field (Figure 13). However, the signature of the young lower continental crust predominates in the set of samples. The Hf data corroborate the significant participation of the crust as the source of the magmas that originated the Morro Redondo complex; however, one zircon grain presented a typically mantle-like $^{176}Hf/^{177}Hf$ ratio, with a model age indicating juvenile mantle melting.

When correlated with other alkaline bodies of the PCCFA, the similarity between lithological units, the geochemical signature of some complexes, and even the variation in ages suggesting the passage of a mantle plume is noted. However, the different models related to the genesis of igneous bodies of the PCCFA consider that these were the product of the evolution of purely mantle magmas. What is currently being discussed is what type of mantle is involved; for example, Ulbrich et al. (2003), Riccomini et al. (2005), and Guarino et al. (2021) consider that the bodies of the PCCFA originated from the partial melting of the lithospheric mantle, while Gordon et al. (2023) consider a strong association with the enriched mantle. What has not been considered is the significant participation of components of the lower crust as a source of magmatism, which was also observed by Silva et al. (2023) in the Soarinho

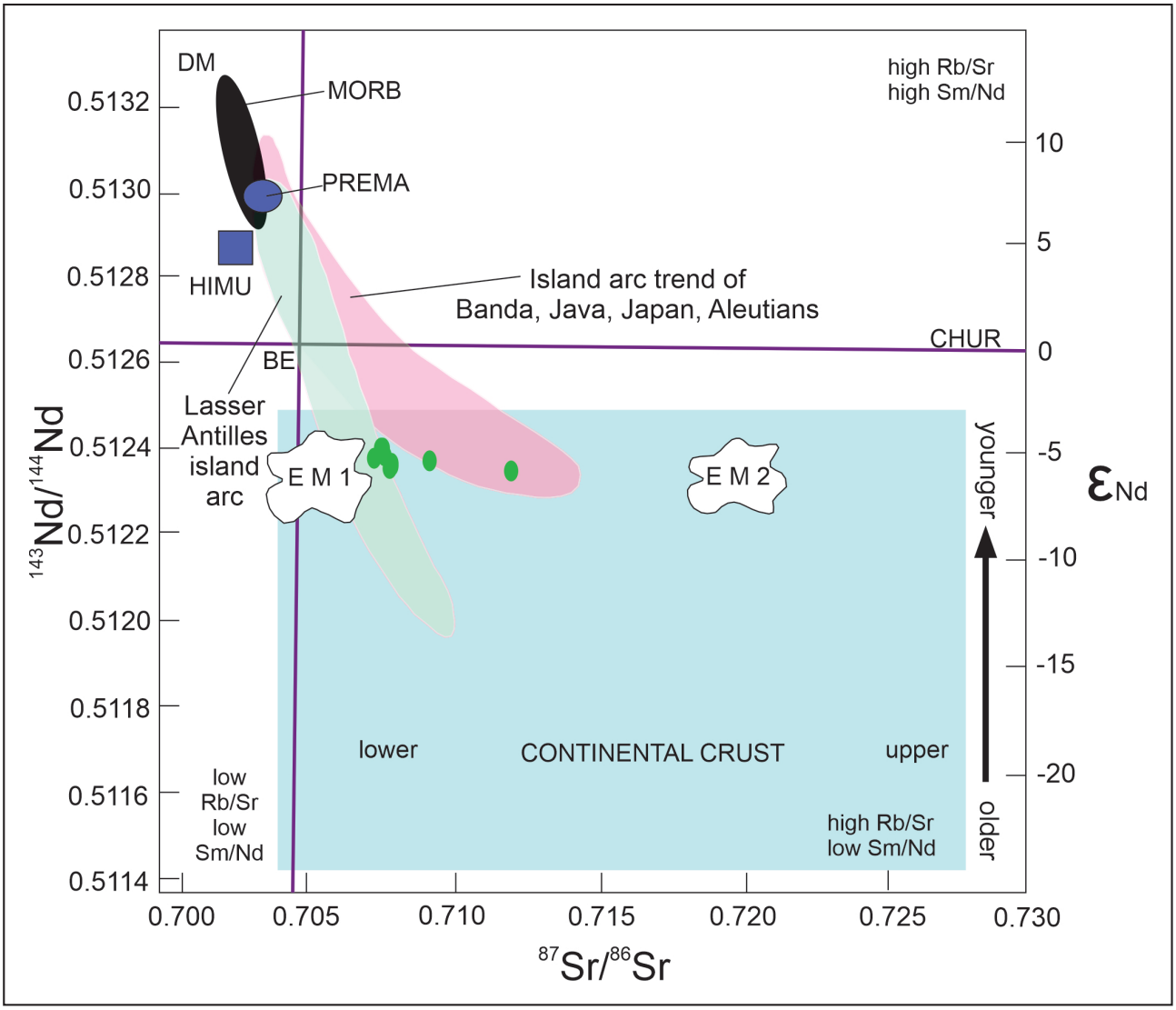

FIGURE 13. Isotopic data $^{87}Sr/^{86}Sr$ vs $^{143}Nd/^{144}Nd$ obtained in this work compared with different isotopic reservoirs. These include the depleted mantle (DM), bulk silicate Earth (BE), enriched mantle (EM1 and EM2), high- μ (U/Pb) (HIMU), and the prevalent mantle (PREMA). Modified from Rollinson and Pease (2021).

complex. Therefore, it can be suggested that, at least for the Morro Redondo complex, the genesis of magmatism involved mantle origin and significant crustal contribution.

6. Conclusions

Based on the investigations presented, our study of the Morro Redondo complex indicates that:

• The association of rocks present in this magmatic complex is like other bodies of the PCCFA, with both plutonic and volcanic rocks present. There is also a predominance of nepheline syenites and alkali feldspar syenites.

• The mineral paragenesis and geochemical signature of the rocks from Morro Redondo demonstrate that these rocks are essentially miaskitic. Geochemical data also indicate a significant crustal contribution to the development of this magmatism.

• The ages obtained using the $^{40}Ar/^{39}Ar$ and U-Pb methodologies are discordant with the regional pattern of decreasing ages of alkaline bodies from west to east.

• The isotopic data point to at least two distinct sources associated with magmatism in the Morro Redondo complex.

Acknowledgements

The authors would like to thank the funding agencies. Guilherme Loriato Potratz would like to thank Fundação Carlos Chagas Filho de Amparo à Pesquisa do Estado do Rio de Janeiro for his postdoctoral scholarship, process number E26-204.530/2021 and E26-204.531/2021. Mauro Cesar Geraldes thanks the National Council for Scientific and Technological Development (CNPq) for the research grant (process nº 301470/2016-2).

Authorship credits

Author	Study design/ Conceptualization	Investigation/Data acquisition	Data Interpretation/ Validation	Writing	Review/ Editing	Supervision/ Project administration
CEM						
AMSFMS						
FJ						
MCG						
GLP						

References

Almeida F.F.M. 1971. Condicionamento tectônico do magmatismo alcalino Mesozóico do sul do Brasil e do Paraguai oriental. Anais da Academia Brasileira de Ciências, 43(3-4), 835-836. Available on line at: http://memoria.bn.br/DocReader/158119/17871 / (accessed on 27 March 2024).

Almeida F.F.M. 1972. Tectono-magmatic activation of the South American platform and associated mineralization. In: International Geological Congress, 24, 339-346.

Almeida F.F.M. 1991. O alinhamento magmático de Cabo Frio. In: Simpósio de Geologia do Sudeste, 2, 423-428. Available on line at: http://acervo.cprm.gov.br/rpi_cprm/docreaderNET/docreader.aspx?bib=Anais&PagFis=58724 / (accessed on 27 March 2024).

Almeida F.F.M., Carneiro C.D.R., Mizusaki A.M.P. 1996. Correlação do magmatismo das bacias da margem continental brasileira com o das áreas emersas adjacentes. Revista Brasileira de Geociências, 26(3), 125-138. https://doi.org/10.25249/0375-7536.19963125138

Alves E.C., Maia M., Sichel S.E., Campos C.M.P. 2006. Zona de fratura de Vitória-Trindade no Oceano Atlântico sudeste e suas implicações tectônicas. Revista Brasileira de Geofísica, 24(1), 117-127. https://doi.org/10.1590/S0102-261X2006000100009. Available on line at: https://www.scielo.br/j/rbg/a/ZTWh86zhhJCp8PdmxsKSCvL / (accessed on 27 March 2024).

Amaral G., Bushee J., Cordani U.G., Kawashita K., Reynolds J.H. 1967. Potassium-argon ages of alkaline rocks from southern Brazil. Geochimica et Cosmochimica Acta, 31(2), 117-142. https://doi.org/10.1016/S0016-7037(67)80041-3

Andersen T., Elburg M., Erambert M. 2017. The miaskitic-to-agpaitic transition in peralkaline nepheline syenite (white foyaite) from the Pilanesberg Complex, South Africa. Chemical Geology, 455, 166-181. https://doi.org/10.1016/j.chemgeo.2016.08.020

Araújo A.L. 1995. Geologia, geoquímica e petrologia das rochas alcalinas da ilha do Cabo Frio e das áreas continentais adjacentes, Arraial do Cabo-RJ. MSc Dissertation, Departamento de Geologia e Geofísica, Universidade Federal Fluminense, Niterói, 114 p.

Blichert-Toft J., Albarède F. 1997. The Lu-Hf isotope geochemistry of chondrites and the evolution of the mantle-crust system. Earth and Planetary Science Letters, 148(1-2), 243-258. https://doi.org/10.1016/S0012-821X(97)00040-X

Boynton W.V. 1984. Cosmochemistry of the rare earth elements: meteorite studies. In: Henderson P. (ed.). Rare earth element geochemistry. Developments in Geochemistry, 2. Amsterdam, Elsevier, p. 63-114. https://doi.org/10.1016/B978-0-444-42148-7.50008-3

Brotzu P., Beccaluva L., Conte A., Fonseca M., Gomes C.B., Leong L., Macciotta G., Mansur R.L., Morbidelli L., Ruberti E., Sígolo J.B., Traversa J., Valença J. 1989. Petrological and geochemical studies of alkaline rocks from continental Brazil. 8. The syenitic intrusion of Morro Redondo, RJ. Geochimica Brasiliensis, 3(1), 63-80. Available on line at: https://www.geobrasiliensis.org.br/geobrasiliensis/article/view/25 / (accessed on 27 March 2024.

Brotzu P., Barbieri M., Beccaluva L., Garbarino C., Gomes C.B., Macciotta G., Melluso L., Morbidelli L., Ruberti E., Sígolo J.B. 1992. Petrology and geochemistry of the Passa Quatro alkaline complex, southeastern Brazil. Journal of South American Earth Sciences, 6(4), 237-252. https://doi.org/10.1016/0895-9811(92)90044-Y

Brotzu P., Gomes C.B., Melluso L., Morbidelli L., Morra V., Ruberti E. 1997. Petrogenesis of coexisting SiO2-undersaturated to SiO2-oversaturated felsic igneous rocks: the alkaline complex of Itatiaia, southeastern Brazil. Lithos, 40(2-4), 133-156. https://doi.org/10.1016/S0024-4937(97)00007-8

Brotzu P., Melluso L., D'Amelio F., Lustrino M. 2005. Potassic dykes and intrusions of the Serra do Mar igneous province (SE Brazil). In: Comin-Chiaramonti P., Gomes C.B. (eds.). Mesozoic to Cenozoic alkaline magmatism in the Brazilian Platform. São Paulo, EdUSP, p. 443-472. Available on line at: https://www.livrosabertos.edusp.usp.br/edusp/catalog/book/6 / (accessed on 27 March 2024).

Brotzu P., Melluso L., Bannio L., Gomes C.B., Lustrino M., Morbidelli L., Morra V., Ruberti E., Tassinari C., D'Antonio M. 2007. Petrogenesis of the Early Cenozoic potassic alkaline complex of Morro de São João, southeastern Brazil. Journal of South American Earth Sciences, 24(1), 93-115. https://doi.org/10.1016/j.jsames.2007.02.006

Chiessi C.M. 2004. Tectônica cenozóica do Maciço Alcalino de Passa Quatro (SP-MG-RJ). MSc Dissertation, Instituto de Geociências, Universidade de São Paulo, São Paulo, 116 p. https://doi.org/10.11606/D.44.2004.tde-10042014-161924

DePaolo D.J. 1988. Neodymium isotope geochemistry: an introduction. Berlin, Springer Verlag, 187 p.

Enrich G.E.R., Azzone R.G., Ruberti E., Gomes C.B., Comin-Chiaramonti P. 2005. Itatiaia, Passa Quatro and São Sebastião Island, the major alkaline syenitic complexes from the Serra do Mar region. In: Comin-Chiaramonti P., Gomes C.B. (eds.). Mesozoic to Cenozoic alkaline magmatism in the Brazilian Platform. São Paulo, EdUSP, p. 419-441. Available on line at: https://repositorio.usp.br/item/001673275 / (accessed on 8 April 2024).

Ferrari A.L. 2001. Evolução tectônica do Graben da Guanabara. PhD Thesis, Instituto de Geociências, Universidade de São Paulo, São Paulo, 449 p.

Geraldes M.C., Motoki A., Costa A., Mota C.E., Mohriak W.U. 2013.

Geochronology (Ar/Ar and K-Ar) of the South Atlantic post-break-up magmatism. In: Mohriak W.U., Danforth A., Post P.J., Brown D.E., Tari G.C., Nemčok M., Sinha S.T. Conjugate divergent margins. Special Publications, 369. London, Geological Society, p. 41-74. https://doi.org/10.1144/SP369.21

Gomes C.B., Comin-Chiaramonti P. 2005. An introduction to the alkaline and alkaline-carbonatitic magmatism in and around the Paraná Basin. In: Comin-Chiaramonti P., Gomes C.B. (eds.). Mesozoic to Cenozoic alkaline magmatism in the Brazilian Platform. São Paulo, EdUSP, p. 21-29. Available on line at: https://repositorio.usp.br/item/001673275 / (accessed on 8 April 2024).

Gordon A.C., Santos A.C., Caitano G.R., Stanton N., Mohriak W.U. 2023. Magmatic cycles in Santos Basin (SE Brazil): geochemical characterization and magmatic sources. Journal of South American Earth Sciences, 126, 104323. https://doi.org/10.1016/j.jsames.2023.104323

Guarino V., de' Gennaro R., Melluso L., Ruberti E., Azzone R.G. 2019. The transition from miaskitic to agpaitic rocks, as highlighted by the accessory phase assemblages in the Passa Quatro alkaline complex (Southeastern Brazil). The Canadian Mineralogist, 57(3), 339-361. https://doi.org/10.3749/canmin.1800073

Guarino V., Lustrino M., Zanetti A., Tassinari C.C.G., Ruberti E., de' Gennaro R., Melluso L. 2021. Mineralogy and geochemistry of a giant agpaitic magma reservoir: the Late Cretaceous Poços de Caldas potassic alkaline complex (SE Brazil). Lithos, 398-399, 106330. https://doi.org/10.1016/j.lithos.2021.106330

Koppers A.A.P. 2002. ArArCALC-software for 40Ar/39Ar age calculations. Computers & Geosciences, 28(5), 605-619. https://doi.org/10.1016/S0098-3004(01)00095-4

Le Bas M.J., Le Maitre R.W., Streckeisen A., Zanettin B. 1986. A chemical classification of volcanic rocks based on the total alkali-silica diagram. Journal of Petrology, 27(3), 745-750. https://doi.org/10.1093/petrology/27.3.745

Lee J.-Y., Marti K., Severinghaus J.P., Kawamura K., Yoo H.-S., Lee J.B., Kim J.S. 2006. A redetermination of the isotopic abundance of atmospheric Ar. Geochimica et Cosmochimica Acta, 70(17), 4507-4512. https://doi.org/10.1016/j.gca.2006.06.1563

Ludwig K.R. 2003. User's manual for Isoplot/Ex, version 3.00: a geochronological toolkit for Microsoft Excel. Special Publication, n. 4. Berkeley, Berkeley Geochronology Center, 74 p.

Machado N., Simonetti A. 2001. U–Pb dating and Hf isotopic composition of zircons by laser ablation-MC-ICP-MS. In: Sylvester P.J. (ed.). Laser-ablation-ICPMS in the Earth Sciences: principles and applications. Short Course, v. 29. Ottawa, Mineralogical Association of Canada, p. 121-146.

Melluso L., Guarino V., Lustrino M., Morra V., de' Gennaro R. 2017. The REE- and HFSE-bearing phases in the Itatiaia alkaline complex (Brazil) and geochemical evolution of feldspar-rich felsic melts. Mineralogical Magazine, 81(2), 217-250. https://doi.org/10.1180/minmag.2016.080.122

Montes-Lauar C.R. 1988. Estudo paleomagnético dos maciços alcalinos de Poços de Caldas, Passa Quatro e Itatiaia. MSc Dissertation, Instituto de Geociências, Universidade de São Paulo, São Paulo, 101 p.

Mota C.E., Geraldes M.C., Sousa M.A., Mane M.A. 2012. Estrutura subsuperficial do Complexo Alcalino do Mendanha, Rio de Janeiro, por integração de dados geológicos e gravimétricos. REM: Revista da Escola de Minas, 65(4), 491-499. https://doi.org/10.1590/S0370-44672012000400009

Motoki A., Sichel S.E., Soares R., Aires J.R., Savi D.C., Petrakis G.H., Motoki K.F. 2008. Rochas piroclásticas de preenchimento de condutos subvulcânicos do Mendanha, Itaúna e ilha de Cabo Frio, RJ, e seu processo de formação com base no modelo de implosão de conduto. Geociências, 27(4), 451-467.

Motoki A., Sichel S.E., Vargas T., Aires J.R., Iwanuch W., Mello S.L.M., Motoki K.F., Silva S., Balmant A., Gonçalves J. 2010. Geochemical evolution of the felsic alkaline rocks of Tanguá and Rio Bonito intrusive bodies, state of Rio de Janeiro, Brazil. Geociências, 29(3), 291-310.

Motoki A., Geraldes M.C., Iwanuch W., Vargas T., Motoki K.F., Balmant A., Ramos M.N. 2012. The pyroclastic dyke and welded crystal tuff of the Morro dos Gatos alkaline intrusive complex, state of Rio de Janeiro, Brazil. REM: Revista da Escola de Minas, 65(1), 35-45. https://doi.org/10.1590/S0370-44672012000100006

Motoki A., Araújo A.L., Sichel S.E., Geraldes M.C., Jourdan F., Motoki K.F., Silva S. 2013. Nepheline syenite magma differentiation with continental crustal assimilation for the Cabo Frio island intrusive complex, state of Rio de Janeiro, Brazil. Geociências, 32(2), 195-218.

Paquette J.-L., Mergoil-Daniel J. 2009. Origin and U–Pb dating of zircon-bearing nepheline syenite xenoliths preserved in basaltic tephra (Massif Central, France). Contributions to Mineralogy and Petrology, 158(2), 245-262. https://doi.org/10.1007/s00410-009-0380-y

Renne P.R., Mundil R., Balco G., Min K., Ludwig K.R. 2010. Joint determination of 40K decay constants and 40Ar*/40K for the Fish Canyon sanidine standard, and improved accuracy for 40Ar/39Ar geochronology. Geochimica et Cosmochimica Acta, 74(18), 5349-5367. https://doi.org/10.1016/j.gca.2010.06.017

Renne P.R., Balco G., Ludwig K.R., Mundil R., Min K. 2011. Response to the comment by W.H. Schwarz et al. on "Joint determination of 40K decay constants and 40Ar*/40K for the Fish Canyon sanidine standard, and improved accuracy for 40Ar/39Ar geochronology" by P.R. Renne et al. (2010). Geochimica et Cosmochimica Acta, 75(17), 5097-5100. https://doi.org/10.1016/j.gca.2011.06.021

Riccomini C., Velázquez V.F., Gomes C.B. 2005. Tectonic controls of the Mesozoic and Cenozoic alkaline magmatism in Central-Southeastern Brazilian Platform. In: Comin-Chiaramonti P., Gomes C.B. (eds.). Mesozoic to Cenozoic alkaline magmatism in the Brazilian Platform. São Paulo, Edusp, 31-56. Available on line at: https://www.livrosabertos.edusp.usp.br/edusp/catalog/book/6 / (accessed on 8 April 2024).

Rollinson H., Pease V. 2021. Using geochemical data: to understand geological processes. 2nd ed. Cambridge, Cambridge University Press, 358 p.

Rosa P.A.S., Ruberti E. 2018. Nepheline syenites to syenites and granitic rocks of the Itatiaia Alkaline Massif, Southeastern Brazil: new geological insights into a migratory ring Complex. Brazilian Journal of Geology, 48(2), 347-372. https://doi.org/10.1590/2317-4889201820170092

Sadowski G.R., Dias Neto C.M. 1981. O lineamento sismo-tectônico de Cabo Frio. Revista Brasileira de Geociências, 11(4), 209-212. Available on line at: http://bjg.siteoficial.ws/1981/n4/sadowski.pdf / (accessed on 8 April 2024).

Santos A.C., Hackspacher P.C. (eds.). 2021. Meso-Cenozoic Brazilian offshore magmatism: geochemistry, petrology, and tectonics. London, Academic Press, 483 p. https://doi.org/10.1016/C2019-0-05400-3

Shand S.J. 1943. Eruptive rocks: their genesis, composition, classification, and their relation to ore-deposits, with a chapter on meteorite. 2nd ed. New York, John Willey & Sons, 444 p.

Sichel S.E., Esperança S., Motoki A., Maia M., Horan M.F., Szatmari P., Alves E.C., Mello S.L.M. 2008. Geophysical and geochemical evidence for cold upper mantle beneath the Equatorial Atlantic Ocean. Revista Brasileira de Geofísica, 26(1), 69-86. https://doi.org/10.1590/S0102-261X2008000100006

Sígolo J.B., Rubertí E., Gomes C.B. 1992. O complexo alcalino de Passa Quatro: dados geológicos preliminares. Boletim IG-USP. Publicação Especial, 12, 109-111. https://doi.org/10.11606/issn.2317-8078.v0i12p109-111

Silva D.A. 2019. Geoquímica e geocronologia (U-Pb e Lu-Hf) das intrusões alcalinas félsicas de Soarinho, Tanguá, Rio Bonito e Tinguá: implicações sobre as fontes do magmatismo alcalino no estado do Rio de Janeiro. PhD Thesis, Centro de Tecnologia e Ciências, Universidade do Estado do Rio de Janeiro, Rio de Janeiro, 186 p. Available on line at: http://www.bdtd.uerj.br/handle/1/6995 / (accessed on 8 April 2024).

Silva D.A., Motoki A., Santos A.C., Mendes J., Jourdan F., Geraldes M.C., Lana C.C. 2020. Multiple processes of geochemical evolution for the alkaline rocks of Rio Bonito intrusive complex, Rio de Janeiro state, Brazil: 40Ar/39Ar and U-Pb ages and Lu-Hf isotopes on zircon and constraints on crustal signature. Geologia USP. Série Científica, 20(4), 213-234. https://doi.org/10.11606/issn.2316-9095.v20-151049

Silva D.A., Potratz G.L., Geraldes M.C. 2023. Geochemistry and geochronology (U-Pb and Lu-Hf) of the Soarinho Alkaline Massif (Brazil): implications on mantle versus crustal signature of syenitic magma. Minerals, 13(7), 904. https:// doi.org/10.3390/min13070904

Sun S.-S., McDonough W.F. 1989. Chemical and isotopic systematics of oceanic basalts: implications for mantle composition and processes. In: Saunders A.D., Norry M.J. (eds.). Magmatism in the ocean basins. Special Publications, v. 42. London, Geological Society, p. 313-345. https://doi.org/10.1144/GSL.SP.1989.042.01.19

Tera F., Wasserburg G.J. 1972. U-Th-Pb systematic in three Apolo 14 basalts and the problem of initial Pb in lunar rocks. Earth and Planetary Science Letters, 14(3), 281-304. https://doi.org/10.1016/0012-821X(72)90128-8

Thomaz Filho A., Cesero P., Mizusaki A.M., Leão J.G. 2005. Hot spot volcanic tracks and their implications for south American plate motion, Campos basin (Rio de Janeiro state), Brazil. Journal of South American Earth Sciences, 18(3-4), 383-389. https://doi.org/10.1016/j.jsames.2004.11.006

Thompson R.N., Gibson S.A., Mitchell J.G., Dickin A.P., Leonardos O.H., Brod J.A., Greenwood J.C. 1998. Migrating Cretaceous-Eocene magmatism in the Serra do Mar alkaline province, SE Brazil: melts from the deflected Trindade mantle plume? Journal of Petrology, 39(8), 1493-1526. https://doi.org/10.1093/petroj/39.8.1493

Tupinambá M., Teixeira W., Heilbron M. 2012. Evolução tectônica e magmática da Faixa Ribeira entre o Neoproterozóico e Paleozóico inferior na região serrana do estado do Rio de Janeiro, Brasil. Anuário do Instituto de Geociências - UFRJ, 35(2), 140-151. https://doi.org/10.11137/2012_2_140_151

Ulbrich H., Demaiffe D., Vlach S.R.F., Ulbrich M.N.C. 2003. Geochemical and Sr, Nd and Pb isotope signatures of phonolites and nepheline syenites from the Poços de Caldas alkaline massif, southeastern Brazil. In: South American Symposium of Isotope Geology, 4, 698-701.

Valeriano C.M., Tupinambá M., Simonetti A., Heilbron M., Almeida J.C.H., Eiraldo L.G. 2011. U-Pb LA-MC-ICPMS geochronology of Cambro-Ordovician post-collisional granites of the Ribeira belt, Southeast Brazil: Terminal Brasiliano magmatism in central Gondwana supercontinent. Journal of South American Earth Sciences, 32(4), 416-428. https://doi.org/10.1016/j.jsames.2011.03.003

VanDecar J.C., James D.E., Assumpção M. 1995. Seismic evidence for a fossil mantle plume beneath South America and implications for plate driving forces. Nature, 378(6552), 25-31. https://doi.org/10.1038/378025a0

Vervoort J.D., Patchett P.J. 1996. Behavior of hafnium and neodymium isotopes in the crust: Constraints from Precambrian crustally derived granites. Geochimica et Cosmochimica Acta, 60(19), 3717-3733. https://doi.org/10.1016/0016-7037(96)00201-3

Vlach S.R.F., Ulbrich H.H.G.J., Ulbrich M.N.C., Vasconcelos P.M. 2018. Melanite-bearing nepheline syenite fragments and 40Ar/39Ar age of phlogopite megacrysts in conduit breccia from the Poços de Caldas Alkaline Massif (MG/SP), and implications. Brazilian Journal of Geology, 48(2), 391-402. https://doi.org/10.1590/2317-4889201820170095

Zalán P.V., Oliveira J.A.B. 2005. Origem e evolução estrutural do sistema de riftes Cenozóicos do Sudeste do Brasil. Boletim de Geociências da Petrobras, 13(2), 269-300.